Journal of New Technology and Materials (JNTM)
J. New Technol. Mater.
Vol. 12, N°02 (2022)89-96

OEB Univ. Publish. Co.

The effect of uniaxial stress on structural and electronic properties in half-heusler FeVSb: *ab-initio* study

B. Benchehida[a,b], H. Abbassa[a,b], S. Meskine[a] and E. H. Abbes[a,b,*]

[a]*Elaboration and Characterization Physical Mechanics and Metallurgical of Materials Laboratory (ECP3M) Faculty of science and technology, Electrical Engineering Department,Abdelhamid Ibn Badis University-Mostaganem, Route nationale N°11, Kharrouba, 27000 Mostaganem, Algeria.*
[b]*Department of Physics, Faculty of Exact Sciences and Computer Science – Mostaganem, Algeria.*

*Corresponding author, email : a27habib@gmail.com

Received date: Oct. 2, 2022 ; accepted date: Nov. 5, 2022

Abstract

From the first-principles calculations based on density functional theory with the generalized gradient approximation, structural, electronic and optical properties of FeVSb, half Heusler compound are calculated within the framework to understand the effect of both uniaxial and hydrostatic stress. The calculated total energy variation indicates that the ground state corresponds to the cubic structure for none magnetic (NM) state. The material undergoes a structural phase transition under a uniaxial pressure of 0.5 GPa, it is found very inferior than that under hydrostatic pressure (Bo Kong et al., Physica B. 406 (2011) 3003-3010). From both band structure and density of states, half Heusler alloy FeVSb is found to be a semiconductor with an energy gap of 0.34 eV. The study of the optical properties shows that the uniaxial stress contributes to the weakening of the optical properties of this material.

Keywords: Electronic; FP-LAPW calculations; Half Heusler; thermoelectric.

1. Introduction

Since 1903 (the first discovery of Heusler alloys series with cubic structure, *L2*), more than a thousand materials have been identified as Heusler alloys [1]. This kind of compound is currently suitable material for many applications, among which, we cite half metals [2,3] (as ideal electrode compounds for spintronic devices), superconductivity [4], shape memory alloys [5-7], and thermoelectric compounds [8-10]. In the general case, full Heusler alloys crystallize in the cubic $AlCu_2Mn$-type ($L2_1$ structure) with the space group $Fm\bar{3}m$ (SG 225) [11]. Where, X, Y and Z atoms are placed on the Wyckoff positions 8c (1/4,1/4,1/4), 4a (0,0,0) and 4b (1/2,1/2,1/2), respectively [12]. The $L2_1$ structure presents the result of four interpenetrating sub-lattices (fcc) [13]. In some rare cases, full Heusler compounds crystallize in the hexagonal structure [14] ($D0_{19}$ modified) or the tetragonal structure [15] ($D0_{22}$). When the number of 3d electrons of Y atom is more than that of X atom, $CuHg_2Ti$-type structure with the space group observed, where X atoms occupy the nonequivalent 4a (0,0,0) and 4c (1/4,1/4,1/4) positions. At the same time, Y and Z atoms are located on 4b (1/2,1/2,1/2) and 4d (3/4,3/4,3/4) positions, respectively [16].

Half Heusler compounds with the chemical formula XYZ [17] are derived from the $CuHg_2Ti$-type structure when 4b (1/2,1/2,1/2) is empty, known as $C1_b$ structure. For rare cases, these compounds can crystallize in a hexagonal structure (space group $P6_3/mmc$, No. 194), where two atomic arrangements are possible [18]. In atomic configuration I, Fe atoms are located at *2d* (1/3, 2/3, 3/4) sites, V atoms are located at *2a* (0, 0, 0) sites and Sb atoms are located at *2c* (1/3, 2/3, 1/4) sites, for the second configuration (hexagonal II) Fe and V atoms swap their positions.

In this work, we have investigated the half Heusler compound FeVSb, in order to understand the effect of uniaxial stress on the structural, electronic and optical properties.

2. Computational Method

In this work, our electronic structure calculations were performed using the self-consistent full-potential linearized augmented plane wave (FPLAPW) method [19] which is integrated into WIEN2K code [20] within DFT, density functional theory. As exchange-correlation correction, it was used the Perdewe-Burkee-Ernzerhof generalized gradient approximation (GGA) [21,22], of which the space is divided into non-overlapping muffin-tin (MT) spheres that are separated by an interstitial region. Inside these spheres, basis functions are expanded into spherical harmonic functions and Fourier series for the interstitial area. In the present work, muffin-tin sphere radii were 2.10 a.u. for Fe and V, 2.25 a.u. for Sb. The convergence of the basis was controlled by $R_{MT}K_{max}$ = 9 (cutoff parameter), where RMT is the smallest of the MT sphere radii, and Kmax is the largest reciprocal lattice vector used in the plane wave expansion. The magnitude of the most significant vector in charge density Fourier expansion (Gmax) was 12. The value of cutoff energy (which defines the separation of valence and core states) was chosen as -6 Ry. The energy convergence was selected as 0.0001Ry during self-consistency cycles. In Brillouin zone integration (BZ), using the tetrahedron method [20] with 104 particular k points (for cubic phase) and 180 unique k points (for hexagonal phase) in the irreducible wedge

(3000 k-points in the full BZ) was used to construct the charge density in each self-consistency step.

3. Results and Discussion

3.1. Structural Properties

To determine the ground state energy for FeVSb half Heusler, we have considered the cubic structure ($C1_b$) often observed in these compounds and the hexagonal structure. Fig. 1 shows the variation of the ground state energy versus volume for FeVSb alloy, where the non-magnetic cubic structure corresponds to the most stable structure.

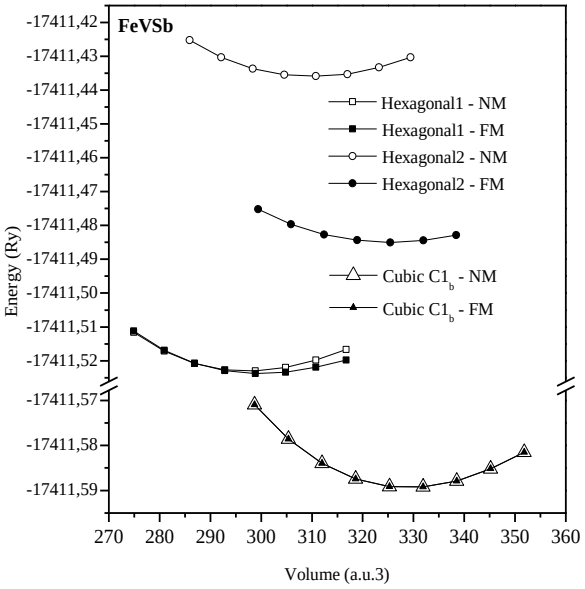

Figure 1. Variation of total energy versus volume for FeVSb half-Heusler alloy.

Using the non-linear fitting with the empirical Murnaghan's equation of states (E-O-S) [23,24], we have determined the ground state's properties. The obtained results for the structural parameters of the studied compound are listed in Table 1, in which the available results of the other calculations are also shown.

$$E(V) = E_0 + \frac{B}{B'(B'+1)}\left[V\left(\frac{V_0}{V}\right)^{B'} - V_0\right] + \frac{B}{B'}(V - V_0) \quad (1)$$

In addition, we have calculated the formation energy E of FeVSb half-Heusler alloy to confirm the possibility of its realization, with the following formula [27]:

$$E_f = E_{\mathrm{FeVSb}}^{total} - (E_{Fe}^{bulk} + E_{\mathrm{V}}^{bulk} + E_{\mathrm{Sb}}^{bulk}) \quad (2)$$

Where $E_{\mathrm{FeVSb}}^{total}$ is the total energy of FeVSb per formula unit, and E_{Fe}^{bulk}, E_{V}^{bulk} and E_{Sb}^{bulk} are the total energies per atom of each element in the bulk for the Fe, V, and Sb, respectively. The negative formation energy (see Table 1) indicates the possibility of formation and even the structural stability of this Heusler compound.

From Table 1, it is clear that our calculated lattice parameter is in good agreement with the other theoretical values.

Table2: Structural parameters, the lattice parameter a in (Å), Bulk modulus B in (GPa) and its first pressure derivative B' and formation energy in (eV) for FeVSb half-Heusler alloy.

FeVSb	cubic structure			
	a (Å)	B_0 (GPa)	B'	E_f (eV)
This work	5.799	163.518	4.297	-0.624
Other Calc. [25]	5.816			
Other Calc. [26]	5.733			

To investigate the effect of pressure on structural properties, we considered two types of pressure, hydrostatic and uniaxial for a range from 0 to 20 GPa. We examined the effect of pressure in order to predict a possible transition. For this purpose, we have calculated and plotted the enthalpy variation as a function of pressure. For hexagonal structure (the target structure), we considered the hydrostatic pressure, while for the ground state structure ($C1_b$) we took the uniaxial pressure.

According to Fig. 2, there is an intersection between the enthalpy variation curves (lines) for both cubic and hexagonal structures under the effect pressure. The uniaxial stress along the z axis causes a phase transition around 0.5 GPa (Fig. 2). We note that a phase transition between cubic and hexagonal structures was also found under hydrostatic stress by B. Kong et *al.* [18], it is around 42 GPa according to a self-consistent calculation based on PP-LAPW code. The large difference can be due to the types of pressures applied (uniaxial in this work and hydrostatic in Ref. [18]) and also to the methods of calculation (FP-LAPW in this work and PP-LAPW in Ref. [18]).

To evaluate the uniaxial stresses, we used the following formula [28,29]:

$$P_z = -\frac{1}{\Omega}\frac{dE_{tot}}{d\delta_z} \quad (3)$$

Where Ω is the relaxed volume of the unit cell, E_{tot} is the total energy and δ_z is the uniaxial stain along z axis.

The obtained result indicates that FeVSb half-Heusler compound has a possibility of phase transformation under the effect of a uniaxial pressure.

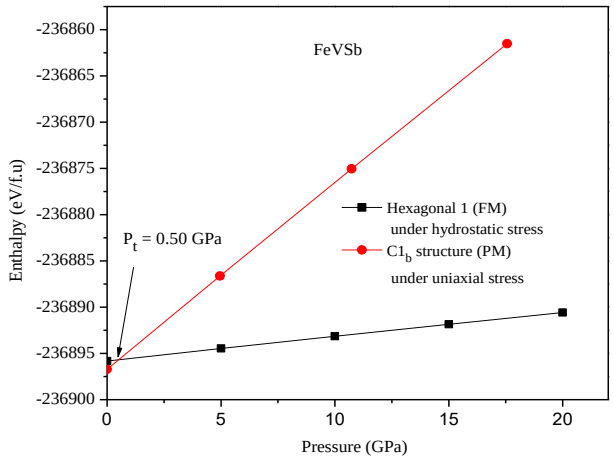

Figure 2. Enthalpy variation as a function of pressure for FeVSb half-Heusler alloy.

3.2. Elastic Properties

From elastic constants calculation, we obtain more information about binding characteristics between adjacent atomic planes and check the structural stability of the studied compound. The elasticity domain defines the characteristics of a solid material (alloy) that undergoes stress, then deforms and returns to its original shape after stress ceases [30].

For a cubic structure, symmetry reduces the elastic tensor elements to only three independent constants C_{11}, C_{12} and C_{44}. To calculate these coefficients, we used in this work, the strains defined according to Mehl Model [31-33].

The calculated elastic constants C_{ij} (for the ground state) are:

C_{11}= 303.175 GPa, C_{12}= 103.541 GPa and C_{44}= 92.076 GPa.

For any cubic system, elastic constants have to satisfy the following stability criteria [34,35].

$$C_{11} > 0,\ C_{44} > 0,\ C_{11} - C_{12} > 0,\ C_{11} + 2C_{12} > 0. \quad (4)$$

Our calculated values verify all the stability criteria, which indicate a structural stability of FeVSb half-Heusler compound in the cubic phase $C1_b$.

3.3. Phonon Spectra

Phonons have a significant role in several physical properties in solid materials; among these properties, we cite thermal properties, electrical conductivity, Debye temperature, and superconducting temperature [36]. The dispersion relation describes the dependence of the vibration frequency on the wave vector (k),

$$\omega(k) = \sum \omega_i(k) \quad (5)$$

We have used the Phonopy code [37] to calculate and plot the phonon dispersion curves in the present work. FeVSb half-Heusler alloy contains three atoms per unit cell in the cubic $C1_b$ structure, so there are nine branches of dispersion curves. Phonon frequencies can only be calculated in the first Brillouin zone (BZ) with translational symmetry.

$$\omega_i(k + G) = \omega_i(k) \quad (6)$$

Fig. 3 Illustrates the phonon dispersion curves along with some high-symmetry points in the first Brillouin zone. The positive phonon frequencies shown in Fig. 3 confirm the structural stability of the $C1_b$ phase, as found in elastic constants section.

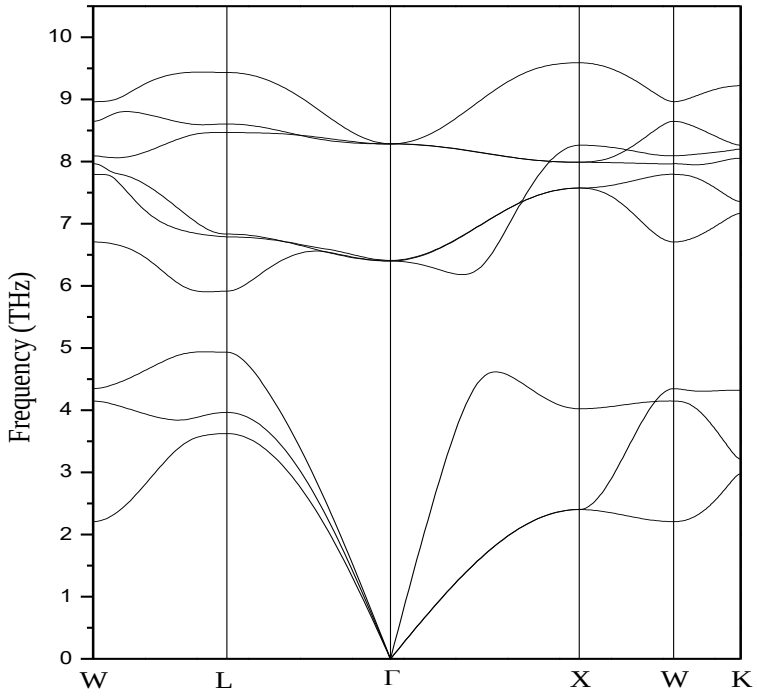

Figure 3. The curves for phonon dispersion of FeVSb half-Heusler alloy along several high-symmetry points.

3.4. Electronic Properties

The band structure and the density of states for the FeVSb compound at the ground state structure are plotted in Fig. 4 and Fig. 5. Our compound has a semiconducting (SC) non-magnetic (NM) behavior, where the energy gap is 0.34 eV. From the calculated D.O.S (Fig. 4), we distinguish four main regions. The first region (bottom valence-band) is dominated by *s*-Sb, while in the second region (-6 eV to -2 eV), the *p*-Sb, *d*-Fe, and *d*-V states dominate. For the third region (upper valence-band), it is clear that only transition metals dominate the DOS by an intense peak around 1 eV consisting of *d*-Fe and *d*-V states. On the other hand, conduction-band (CB) forms the fourth region of D.O.S when the *d*-Fe and *d*-V bands dominate, with a strong peak around 1.5 eV. At the Fermi level E_F, the vanishing of the electronic densities of states for FeVSb half-Heusler alloy indicates a semiconducting (SC) behavior.

The calculated band structures (BS) of the half-Heusler alloy FeVSb at equilibrium lattice constants (ground state) along the higher symmetry directions in the Brillouin zone (BZ) are shown in Fig. 5. None intersection of the bands with the Fermi level reveals the semiconducting nature of half-Heusler alloy FeVSb, with an indirect gap (L → X) about 0.34 eV.

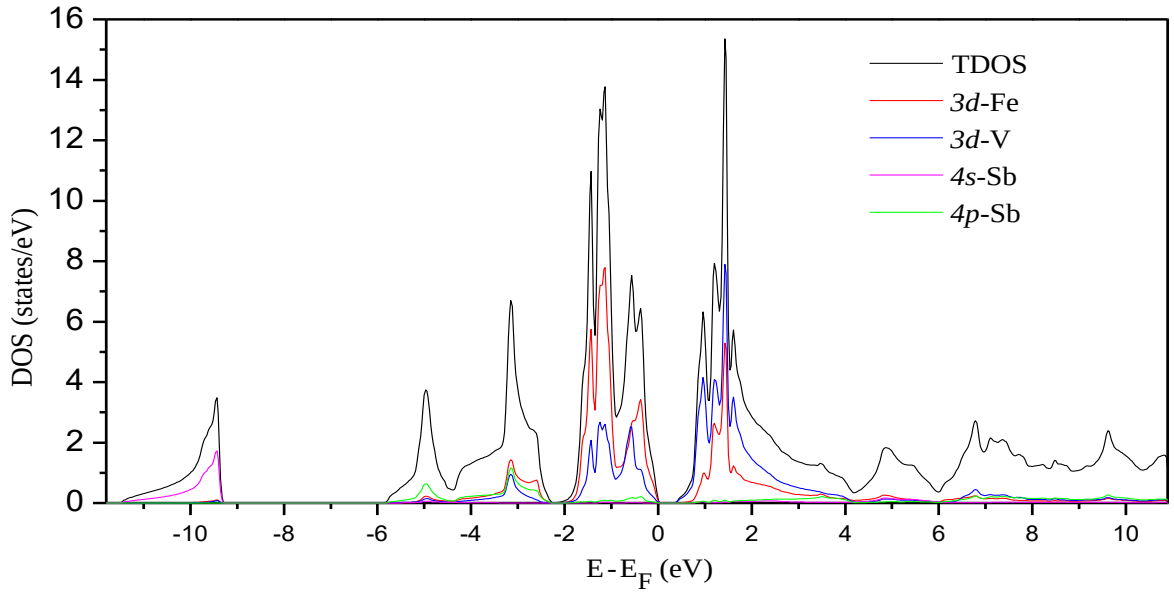

Figure 4. The calculated total/atomic projected densities of states for FeVSb half-Heusler alloy.

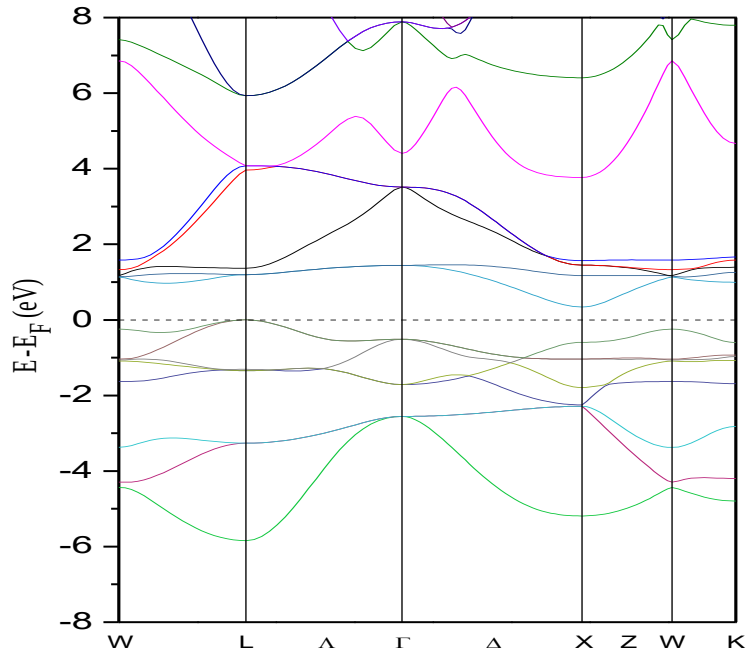

Figure 5. The calculated band structures for FeVSb half-Heusler alloy.

To analyze the contribution of the uniaxial stress on the electronic properties, we only focused our study on the energy gap change. Fig. 6 illustrates the variation of energy gap E_g as a function of uniaxial stress. It is clear that E_g decreases as a polynomial form under the increase of the uniaxial pressure.

3. 5. Optical Properties

In order to determine the energy band structure of a solid material, optical spectroscopy analysis makes a powerful and essential tool [38,39]. To measure quantitatively the performance of FeVSb half-Heusler alloy under uniaxial and hydrostatic stress, we focused our study on three important optical parameters, dielectric function, refraction index and absorption coefficient.

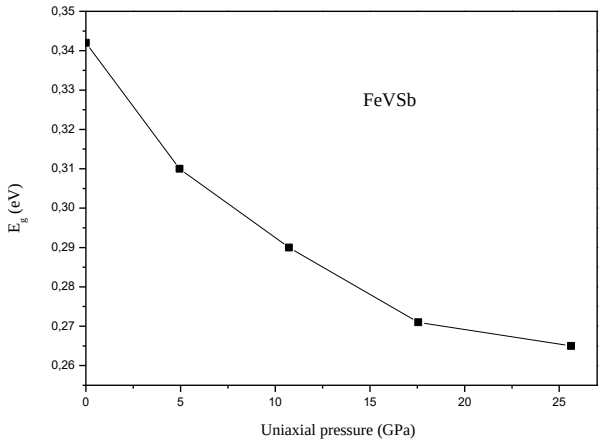

Figure 6. Variation of energy gap (E_g) versus uniaxial pressure for FeVSb half-Heusler alloy.

For a dynamic field, the dielectric function ε (ω) is expressed in a complex function [40], it describes the transition between the valence band and the conduction band according to the response of the material to an electromagnetic radiation:

$$\varepsilon(\omega) = \varepsilon_1 + i\varepsilon_2(\omega) \quad (7)$$

ε_1 (ω) and ε_2 (ω) are the real and imaginary parts of the dielectric function, respectively, where ω represent frequency. These two parts (real and complex) can be calculated via the Kramers-Kronig relation [41].

Both real and imaginary parts of the dielectric function ε (ω), the refraction index n (ω) and the absorption coefficient α (ω) were calculated and plotted under uniaxial strain from 0 to 8 % along the z axis (which corresponds to uniaxial stress from 0 to 25.63 GPa), while for hydrostatic stress, the previous parameters are calculated and plotted for a range from 0 to 20 GPa.

In order to well understand the effect of stress on the dielectric function, we only interested to the intense peak located from 0 to 3.0 eV. The real and imaginary parts of the dielectric function ε (ω) are presented, in the two cases of hydrostatic and uniaxial stresses, in Fig. 7.

Note that in the selected energy range, the real and imaginary parts present two intense peaks located at 1.15 eV and 1.28 eV, respectively.

The variation of the hydrostatic and uniaxial stress gives totally different results for the two cases. We observe that the hydrostatic stress tends to shift the most intense peak for ε_1 (ω) and ε_2 (ω) towards the high energies in a significant way. For ε_1 (ω) the peak at 1.15 eV and ε_2 (ω) the peak at 1.28 eV move to 1.33 eV and 1.50 eV for high pressure, respectively. The shift is done without any significant loss of intensity. The finding is totally different in the case of uniaxial stress along the c axis, where we notice that the latter decreases the intensity without a remarkable shift. The decrease in intensity of the 1.15 eV peak for ε_1 (ω) and 1.28 eV for ε_2 (ω) is estimated to be approximately 20% and 28% respectively.

It is clear that the application of a uniaxial stress along the c axis generates anisotropy of the material which, in our case, changes very little the properties along the *a* and *b* axes.

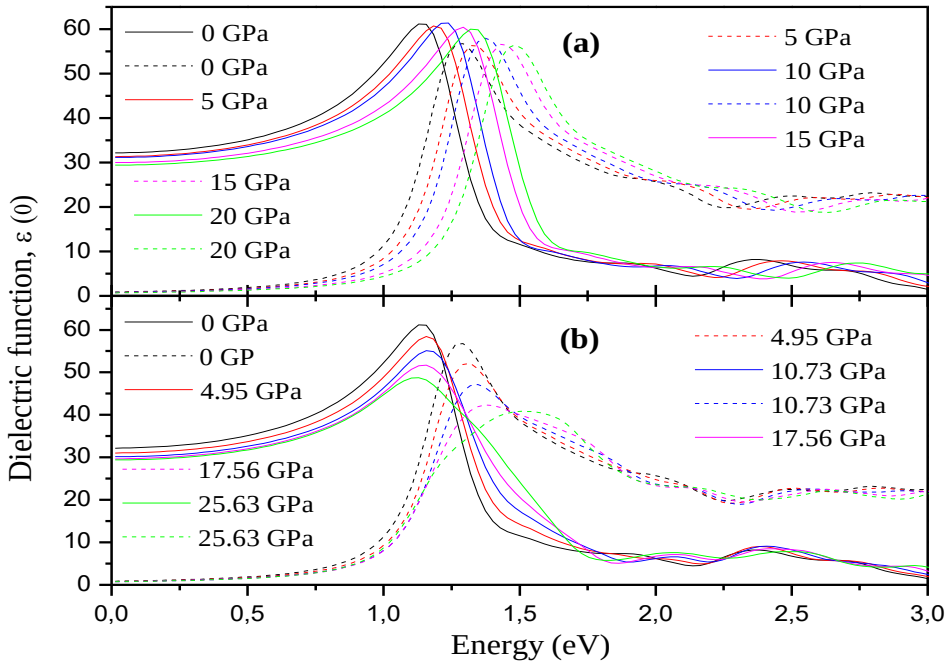

Figure 7. Real (solid lines) and imaginary (dashed lines) parts of the dielectric function ε (0) for FeVSb half-Heusler alloy under hydrostatic stress (a) and uniaxial stress (b).

We also followed the variation of the static dielectric constant ε (0) with the variation of the pressure for the two cases considered Table 2. In this case we noticed that for both cases and in the same way, the static dielectric constant ε (0) decreases with increasing stress.

Table 2: Static dielectric constant ε (0) for hydrostatic (P_h) and uniaxial (P_z) stress in FeVSb half-Heusler alloy, where δ_z (%) is the uniaxial strain along z axis.

Hydrostatic stress		Uniaxial stress		
P_h (GPa)	ε (0)	δ_z (%)	P_z (GPa)	ε (0)
0	32.18	0	0	32.18
5	31.34	2	4.95	31.03
10	31.13	4	10.73	30.14
15	29.97	6	17.56	29.65
20	29.41	8	25.63	29.40

Fig. 8 shows the variation of the absorption coefficient α (ω) with increasing stress for the two considered stress cases.

In the chosen energy range [0; 3.0 eV] and in the unconstrained case, the material has an absorption peak around 1.39 eV which corresponds to a wavelength of 892 nm. After the application of a hydrostatic stress on the material, we observe a shift of the peak towards a value of 1.59 eV which corresponds to a wavelength of 780 nm, with an increase in the absorption coefficient of approximately 15%. In the case of uniaxial stress, behavior of the variation of the absorption coefficient is totally the reverse, with a decrease in absorption of 26% with the disappearance of the peak at energy 1.39 eV. It should be mentioned that the peak in question belongs to the near infrared IR-A range (700 nm - 1400 nm).

The refractive index is shown in Fig. 9, we can clearly see that the refractive index takes values from 3.5 to 4 in the visible range (1.5 eV to 3 eV) in both types of stress. The refractive index shows a strong peak around 1.17 eV (1060 nm) which shifts up to 1.36 eV (912 nm) under 20 GPa hydrostatic stress without any significant change on its value magnitude. By counteracting the uniaxial stress, the magnitude of the peak decreases by nearly 12% with the stress high pressure.

Table 3 shows that the static refractive index n (0) is sensitive to the change in stress in both cases, with a slight decrease in the case of hydrostatic stress and a clear increase in the case of uniaxial stress.

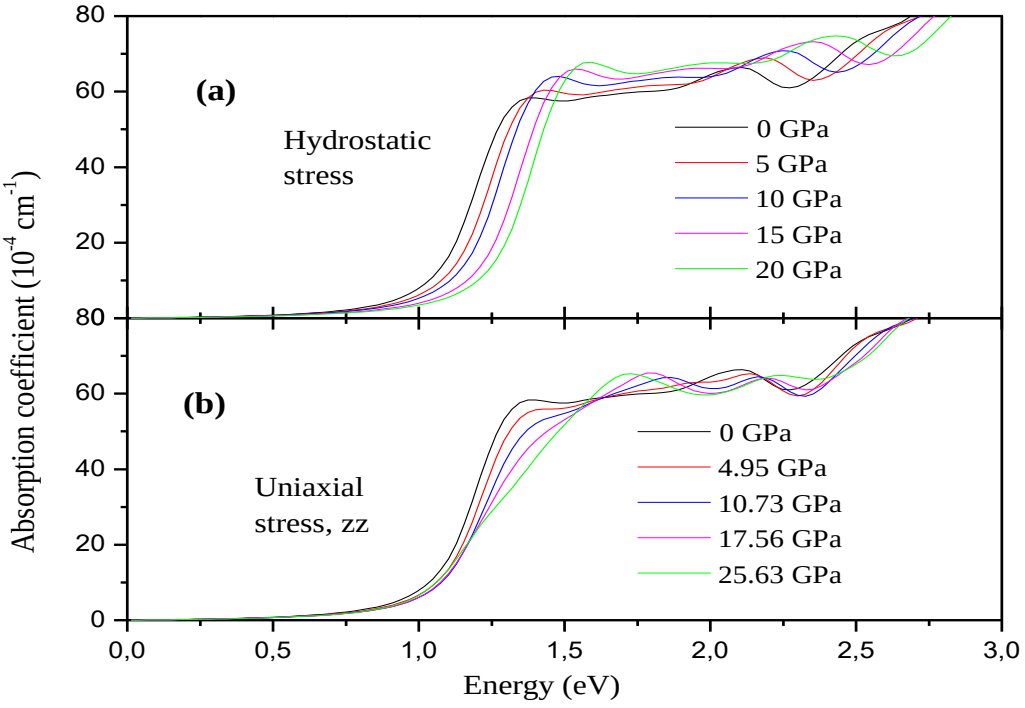

Figure 8. Absorption coefficient for FeVSb half-Heusler alloy under hydrostatic stress (a) and uniaxial stress (b).

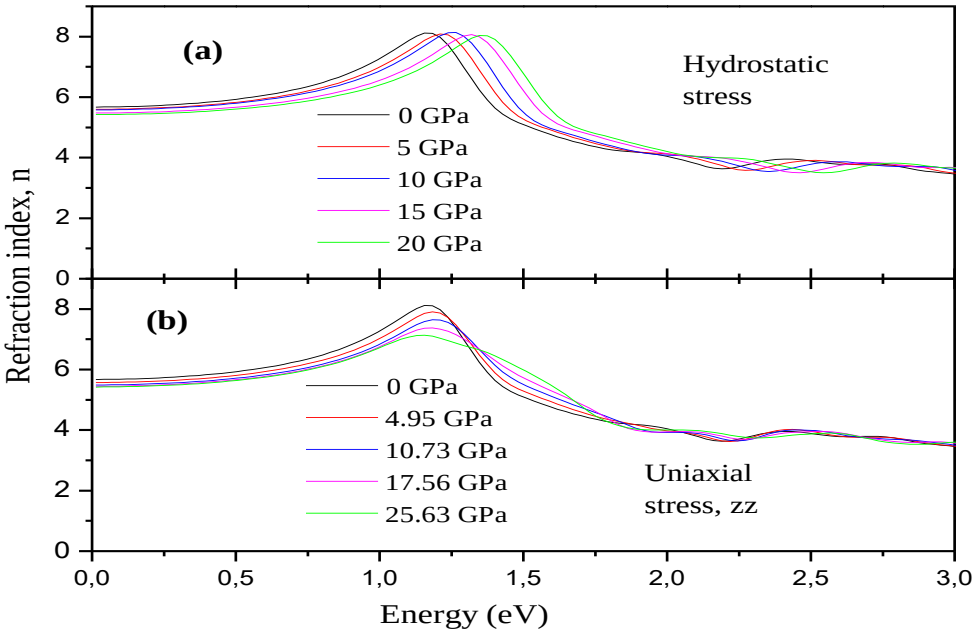

Figure 9. Refraction index for FeVSb half-Heusler alloy under hydrostatic stress (a) and uniaxial stress (b).

Table 3: Refractive index n (0) for hydrostatic (P_h) and uniaxial (P_z) stress in FeVSb half-Heusler alloy, where δ_z (%) is the uniaxial strain along z axis.

Hydrostatic stress		Uniaxial stress		
P_h (GPa)	n (0)	δ_z (%)	P_z (GPa)	n (0)
0	5.67	0	0	5.67
5	5.60	2	4.95	5.70
10	5.60	4	10.73	5.75
15	5.47	6	17.56	5.83
20	5.42	8	25.63	5.94

4. Conclusions

The electronic and structural properties of FeVSb half-Heusler alloy which are investigated under uniaxial stress in this work leads to the following conclusions:

From the results of our calculations based on DFT, the cubic structure $C1_b$ is represented the ground state at the non-magnetic (NM) order. FeVSb half-Heusler alloy has a semiconducting (SC) behavior with an indirect gap of 0.34 eV and keeps its semiconducting behavior for a wide pressure range.

Elastic constants calculation and phonon spectra confirm together the mechanical stability of FeVSb half-alloy.

The material undergoes a structural phase transition under a weak uniaxial pressure of 0.5 GPa from the original cubic structure to the hexagonal II structure.

The hydrostatic stress tends to shift the curves towards high energy (from the infrared towards the visible), with almost the same intensity of the peaks, except for the absorption spectrum where we noticed in addition of the shift, an increase in absorption with increasing hydrostatic stress. On the other hand, uniaxial stress contributes to the weakening of the optical properties of this material.

Acknowledgements

This work is supported by the Algerian national research projects, PRFU/DGRSDT/MESRS-Algeria (project N° B00L02UN270120220001).

References

[1] F. Heusler, Verh. dt. phys. Ges. **5**, 219 (1903).
[2] J. Kübler, A. R. Williams, C. B. Sommers, Phys. Rev. B **28**, 1745 (1983).
[3] I. Galanakis, P. H. Dederichs, and N. Papanikolaou, Phys. Rev. B **66**, 174429 (2002).
[4] B. Wiendlocha, M.J. Winiarski, M. Muras, C. Zvoriste-Walters, J.C. Griveau,S. Heathman, M. Gazda, T. Klimczuk, Phys. Rev. B **91** (2015) 024509.
[5] S. Ağduk and G. Gökoğlu, Eur. Phys. J. B **79**, 509–514 (2011)
[6] Z. H. Liu, M. Zhang, Y. T. Cui, Y. Q. Zhou, W. H. Wang, and G. H. Wu, Appl. Phys. Lett. **82**, 424 (2003).
[7] M. A. Uijttewaal,T. Hickel, J. Neugebauer, M. E. Gruner, and P. Entel, PRL **102**, 035702 (2009)
[8] K. Miyamoto, A. Kimura, K. Sakamoto, M. Ye, Y. Cui, K. Shimada, H. Namatame, M. Taniguchi, S. Fujimori, Y. Saitoh, E. Ikenaga, K. Kobayashi, J. Tadano, and T. Kanomata, Applied Physics Express **1** (2008) 081901
[9] Yasuhiro ONO, Shingo INAYAMA, Hideaki ADACHI and Tsuyoshi KAJITANI, Japanese Journal of Applied Physics Vol. **45**, No. 11, 2006, pp. 8740–8743.
[10] Takeyuki SEKIMOTO, Ken KUROSAKI, Hiroaki MUTA, and Shinsuke YAMANAKA, Japanese

Journal of Applied Physics Vol. **46**, No. 27, 2007, pp. L673–L675.

[11] Hongzhi Luo, Yuepeng Xin, Bohua Liu, Fanbin Meng, Heyan Liu, Enke Liu, Guangheng Wu, *J. Alloy. Comp.* **665** (2016) 180-185.

[12] A. Birsan, *J. Alloy. Comp.* **598** (2014) 230-235.

[13] Lakhan Bainsla, A. K. Yadav, Y. Venkateswara, S. N. Jha, D. Bhattacharyya, K. G. Suresh, *J. Alloy. Comp.* **651**(2015) 509-513.

[14] Parashu Kharel, Y. Huh, V. R. Shah, X. Z. Li, N. Al-Agtash, K. Tarawneh, E. S. Krage, Renat F. Sabirianov, Ralph Skomski, and David J. Sellmyer, JOURNAL OF APPLIED PHYSIICS **111**, 07B101 (2012).

[15] H. Kurt, K. Rode, M. Venkatesan, P. Stamenov, JMD Coey - *Physical Review B*, 2011 - APS

[16] Kandpal HC, Fecher GH, Felser C, J Phys D: Appl Phys **40**, 1507 (2007).

[17] I. Skovsen,L. Bjerg,M. Christensen,E. Nishibori,B. Balke,C. Felserand B. B. Iversen, *Dalton Trans.*, 2010, **39**, 10154–10159

[18] B. Kong, B. Zhu, Y. Cheng, L. Zhang, Q-X. Zeng and X-W. Sun, Physica B. **406** (2011) 3003-3010.

[19] D. J. Singh, "Planes waves, pseudo-potentials and the LAPW method", Kluwer Academic, Boston, 1994.

[20] Blaha P, Schwarz K, Madsen GHK, Hvasnicka D, Luitz J. Technische Universit Wien, ISBN 3-9501031-1-2; 2001.

[21] Perdew JP, Burke K, Wang Y, *Phys. Rev. B. 1996,* **54**, 16533.

[22] Perdew JP, Burke K, Ernzerhof M, *Phys. Rev. Lett. 1996,* **77**, 3865.

[23] F. D. Murnaghan. *Proc. Natl. Acad. Sci. U S A* **30** (1944) 5390.

[24] L. Malakkal, B. Szpunar, J. C. Zuniga, R. K. Siripurapu and J. A. Szpunar, International Journal of Computational Materials Science and Engineering, Vol. **5**, No. 2 (2016) 1650008

[25] J. Tobola, J. Pierre*, Journal of Alloys and Compounds* **296** (2000) 243 –252

[26] Shivprasad S. Shastri and Sudhir K. Pandey, J. Phys.: Condens. Matter **33**, 085704 (2021)

[27] Xiaotian Wang, Zhenxiang Cheng, Yaoxiang Jin, Yang Wu, Xuefang Dai, Guodong Liu, *J. Alloy. Comp.***734** (2018) 329-341

[28] Milan Tomić, Harald O. Jeschke, Rafael M. Fernandes, and Roser Valentí, PHYSICAL REVIEW B **87**, 174503 (2013)

[29] Kazuaki Kobayashi, Materials Transactions, Vol. **46**, No. 6 (2005) pp. 1094 to 1099

[30] H. Rached, D. Rached, R. Khenata, Ali H. Reshak, and M. Rabah, *Phys. Status Solidi B* **246**, No. 7 (2009).

[31] M. J. Mehl, J. E. Osburn, D. A. Papaconstantopoulos, and B. M. Klein, *Phys. Rev. B* **41**, (1990) 10311.

[32] M. J. Mehl, *Phys. Rev. B* **47**, (1993) 2493.

[33] M. J. Mehl, B. M. Klein, and D. A. Papaconstantopoulos, in: Principles Intermetallic Compounds, edited by J. H. West-Brook and R. L. Fleisher, Vol. **1** (Wiley, New York, 1995), chap.9.

[34] O. Baraka, S. Amari and A. Yakoubi, SPIN, Vol. **8**, No. 3 (2018) 1850009

[35] Y. Benaissa Cherif, A. Labdelli, A. Boukortt, H. Abbassa and D. Aimouch, International Journal of ComputationalMaterials Science and Engineering, Vol. **8**, No. 1 (2019) 1850029

[36] TAN Jia-Jin, JI Guang-Fu, CHEN Xiang-Rong and GOU Qing-Quan, Commun. Theor. Phys. **53** (2010) pp. 1160–1166

[37] A. Togo, I. Tanaka, First principles phonon calculations in materials science, Scripta Mater. **108** (2015) 1-5.

[38] B. Amin, R. Khenata, A. Bouhemadou, I. Ahmad and M. Maqbool, Phys. B, 2012, **407**, 2588–2592.

[39] M. Maqbool, B. Amin and I. Ahmad, J. Opt. Soc. Am. B, 2009, **26**, 2181–2184.

[40] H. Luo, R.G. Greene, A.L. Ruoff, Phys. Rev. B **49** (1994) 15341.

[41] M. O'Donnell et al., Acoust. Soc. Am. **69** (1981) 696.